Original Article

JCBFM

Journal of Cerebral Blood Flow & Metabolism
2018, Vol. 38(5) 919–931

DOI: 10.1177/0271678X18755203
journals.sagepub.com/home/jcbfm
SAGE

Quantitative assessment of demyelination in ischemic stroke in vivo using macromolecular proton fraction mapping

Marina Y Khodanovich[1], Alena A Kisel[1], Andrey E Akulov[1,2], Dmitriy N Atochin[1,3,4], Marina S Kudabaeva[1], Valentina Y Glazacheva[1], Michael V Svetlik[1], Yana A Medvednikova[1], Lilia R Mustafina[5] and Vasily L Yarnykh[1,6]

Abstract

A recent MRI method, fast macromolecular proton fraction (MPF) mapping, was used to quantify demyelination in the transient middle cerebral artery occlusion (MCAO) rat stroke model. MPF and other quantitative MRI parameters (T_1, T_2, proton density, and apparent diffusion coefficient) were compared with histological and immunohistochemical markers of demyelination (Luxol Fast Blue stain, (LFB)), neuronal loss (NeuN immunofluorescence), axonal loss (Bielschowsky stain), and inflammation (Iba1 immunofluorescence) in three animal groups ($n = 5$ per group) on the 1st, 3rd, and 10th day after MCAO. MPF and LFB optical density (OD) were significantly reduced in the ischemic lesion on all days after MCAO relative to the symmetrical regions of the contralateral hemisphere. Percentage changes in MPF and LFB OD in the ischemic lesion relative to the contralateral hemisphere significantly differed on the first day only. Percentage changes in LFB OD and MPF were strongly correlated ($R = 0.81$, $P < 0.001$) and did not correlate with other MRI parameters. MPF also did not correlate with other histological variables. Addition of T_2 into multivariate regression further improved agreement between MPF and LFB OD ($R = 0.89$, $P < 0.001$) due to correction of the edema effect. This study provides histological validation of MPF as an imaging biomarker of demyelination in ischemic stroke.

Keywords

Macromolecular proton fraction, middle cerebral artery occlusion, myelin, magnetic resonance imaging, histology

Received 14 August 2017; Accepted 28 December 2017

Introduction

Myelin disruption is a characteristic histopathological feature of the ischemic brain lesion that begins as early as 30 min after the ischemic event[1–3] and further progresses till the formation of a gliotic scar or tissue necrosis.[2,4–7] Remyelination after stroke may serve as an indicator of structural repair and functional recovery of brain tissues.[1,4–9] As such, information about the state of myelin in stroke may play an important role for treatment monitoring and predicting rehabilitation outcomes. To date, there have been no histologically validated noninvasive imaging methods enabling quantitative assessment of demyelination in stroke.

A recently proposed quantitative MRI method, fast macromolecular proton fraction (MPF) mapping,[10,11]

[1]Laboratory of Neurobiology, Tomsk State University, Tomsk, Russian Federation
[2]Institute of Cytology and Genetics, Siberian Branch of the Russian Academy of Sciences, Novosibirsk, Russian Federation
[3]Cardiovascular Research Center, Harvard Medical School, Massachusetts General Hospital, Boston, MA, USA
[4]RASA Center in Tomsk, Tomsk Polytechnic University, Tomsk, Russian Federation
[5]Department of Histology, Embryology and Cytology, Siberian State Medical University, Tomsk, Russian Federation
[6]Department of Radiology, University of Washington, Seattle, WA, USA

Corresponding author:
Marina Y Khodanovich, Tomsk State University, 36 Lenina Ave., Tomsk 634050, Russian Federation.
Email: khodanovich@mail.tsu.ru

has been established as an accurate and simple neuroimaging tool for myelin quantitation in neural tissues[12,13] and demonstrated promising results in pilot clinical studies of multiple sclerosis (MS)[14] and mild traumatic brain injury (mTBI).[15] MPF is a biophysical parameter describing the magnetization transfer (MT) effect and closely correlated with the myelin content according to numerous animal model studies.[12,13,16–19] MT imaging in its various technical implementations showed a promise in quantifying brain tissue damage associated with ischemia at different stages in animal models[20–22] and humans.[23–26] MT imaging techniques vary in their complexity and offer a wide spectrum of applications ranging from simple empirical measurements of the saturation effect in the form of MT ratio[27] to sophisticated image-based multi-parameter fitting procedures intended to generate parametric maps decomposing the MT effect into specific parameters of the two-pool model.[28,29] Due to complex dependence of the MT effect on various changes in molecular and cellular tissue composition, interpretation of quantitative MT parameters is often difficult, particularly in stroke. Although some earlier observed MT abnormalities in brain ischemia could have been attributed to myelin loss,[23,25,26] no direct histological evidence of such a relationship has been established to date. Among MT-based techniques for quantitative tissue characterization, a recently emerged fast MPF mapping method[10,11] offers several practical advantages including clinically acceptable scan time,[14,15] straightforward biophysical interpretation in terms of macromolecular content,[10] insensitivity to magnetic field strength and relaxation properties of tissues,[11,30] high reproducibility,[11,12] and a linear dependence on the myelin content histologically confirmed for normal and demyelinated brain tissues.[12,13]

The objectives of this study were to evaluate the capability of MPF mapping to quantitatively characterize demyelination in stroke at different stages using the rat middle cerebral artery occlusion (MCAO) model, compare MPF performance as a myelin biomarker in stroke with other commonly used quantitative imaging parameters including T_1, T_2, proton density (PD), and apparent diffusion coefficient (ADC), and identify potential confounders in estimation of the myelin content using MPF. The choice of the animal model was motivated by its widespread use, reproducibility, and convenience for MRI applications associated with the animal size and anesthesia tolerance.

Material and methods

Animal procedures

All procedures were performed in accordance with the European Convention for the Protection of Vertebrate Animals used for Experimental and other Scientific Purposes. The experimental protocol was approved by the Bioethical Committees at Tomsk State University and the Institute of Cytology and Genetics of the Siberian Branch of the Russian Academy of Sciences. All experiments described below have been reported following/in compliance with the ARRIVE (Animal Research: Reporting in Vivo Experiments) guidelines. Twenty male Sprague-Dawley rats (weight range 250–270 g) were used. Animals were bred and housed in the specific pathogen-free (SPF) vivarium in individually ventilated cages (one animal per cage, 10/14 light/dark cycle, temperature of 22 to 24°C, humidity of 40 to 50%, water and SPF granulated chow ad libitum). Transient left MCAO was achieved in 15 animals by inserting a nylon filament (diameter 0.185 mm, length 30 mm, diameter with coating 0.39 ± 0.02 mm, coating length 9–10 mm; Doccol, USA) to the origin of the artery for 1 h as described previously.[31] Five sham-operated rats underwent similar manipulations without filament insertion. Animal surgery was performed under isoflurane anesthesia (3% for induction and 1.5–2% for maintenance in combination with 100% oxygen). Quantitative MRI and histological processing were performed on days 1 (MCAO: $n = 5$, sham-operated: $n = 5$), 3 (MCAO: $n = 5$), and 10 (MCAO: $n = 5$) after surgery. Physiological variables including respiration rate, heart rate, body temperature were monitored during the surgical procedure and MR scanning. After MRI, rats were transcardially perfused (4% paraformaldehyde), brains were removed, cryoprotected (sucrose in phosphate buffer solution, 24 h at 10% and 24 h at 20%, 4°C), and stored at −80°C.

Quantitative MRI

In vivo quantitative MRI experiments were performed on an 11.7 T Biospec small-animal MRI scanner (Bruker Biospin, Germany) under isoflurane anesthesia (1.5–2% in oxygen). MPF maps were obtained using the single-point synthetic reference method.[11,30] In brief, the method is based on reconstruction of MPF maps from three source images (MT-, T_1-, and PD-weighted) with correction of B_0[32] and B_1[33] field non-uniformities by voxel-based iterative solution of the pulsed MT equation[10] with a calculated synthetic reference image for data normalization.[11,30] Whole-brain 3D MPF maps were obtained with spatial resolution of $200 \times 200 \times 400\ \mu m^3$ and total scanning time of 35 min using a protocol similar to those previously described.[12,30] The protocol for MPF mapping included the following sequences:

1. MT-weighted spoiled gradient echo (GRE) imaging: repetition time (TR) = 22 ms, echo time (TE) = 2.6 ms, flip angle (FA) = 8°, off-resonance saturation

by the Gaussian pulse with offset frequency of 5 kHz, effective FA = 900°, and duration of 10 ms;
2. T_1-weighted spoiled GRE imaging: TR = 16 ms, TE = 2.6 ms, FA = 16°;
3. PD-weighted spoiled GRE imaging: TR = 16 ms, TE = 2.6 ms, FA = 3°;
4. B_0 mapping based on the dual-TE GRE phase-difference method[32]: TR = 16 ms, TE_1 = 2.4 ms, TE_2 = 4.1 ms, FA = 7°;
5. B_1 mapping based on the dual-TR actual flip-angle imaging (AFI) method[33]: TR_1 = 12 ms, TR_2 = 60 ms, TE = 3.6 ms, FA = 60°.

T_1-weighted and PD-weighted images obtained with the above sequences were also used for the reconstruction of T_1 and PD maps according to the variable flip angle method with B_1 correction.[33] Additionally, maps of macromolecular proton density (MPD) were calculated as a product of parameters MPF and PD.[34] MPD has been suggested in the literature[34] as a parameter less sensitive to the effect of edema than MPF. T_1, PD, MPF, and MPD parametric maps were reconstructed using in-house written C-language software.

T_2 maps were obtained using a multiple spin-echo sequence with TR = 3000 ms, 16 echoes with TE in a range 10–160 ms, slice thickness 0.8 mm, in-plane resolution 200 × 200 μm^2, and scan time 6 min 50 s. For ADC mapping, a single-shot spin-echo diffusion-weighted echo-planar sequence was used with TR/TE = 1500/15.4 ms, three actual b-values of 4.5, 484.2 and 946.5 s/mm^2, slice thickness 0.8 mm, in-plane resolution 300 × 300 μm^2, and scan time 6 min 40 s. T_2 and ADC maps were reconstructed within three-parameter single-exponential models with the noise level as an adjustable parameter using the scanner's software package. All parametric maps were obtained in the coronal plane.

Histology and immunohistochemistry

Brain locations for quantitative histological/immunochemical analysis included ischemic lesion and were defined from −1.92 mm to +1.74 mm from bregma according to a rat brain atlas.[35] Coronal brain sections (10 μm thickness) were prepared using an HM525 cryostat (Thermo Fisher Scientific, Germany) and were stained histologically with Luxol Fast Blue (LFB) for myelin detection and Bielschowsky's silver impregnation (BSI) for the assessment of axonal density. Immunofluorescence staining was used for the assessment of neuronal loss and inflammatory response mediated by activated microglia. Mature neurons were detected by the neuronal marker NeuN using rabbit anti-NeuN primary antibodies (#ABN78; 1:500; Merck Millipore, USA). Microglia were detected by ionized calcium-binding adapter molecule 1 (Iba1) labeling using rabbit anti-Iba1 primary antibodies (#019-19741; 1:500; Wako Pure Chemical Industries, Japan). Secondary donkey anti-rabbit AlexaFlour 488 antibodies (#711-545-152; 1:500; Jackson Immuno-esearch Laboratories, USA) and VECTASHIELD mounting medium (Vector Laboratories, USA) with DAPI (4′,6-diamidino-2-phenylindole) were used for immunofluorescence. Whole-brain sections were photographed using an Axio Imager Z2 microscope (Carl Zeiss, Germany) with AxioVision 4.8 software. Identical imaging parameters (voltage of a microscope lamp and exposure time) were set for all photographed slices. Magnified views of NeuN and Iba1 labeled sections were obtained using an LSM 780 NLO laser confocal microscope (Carl Zeiss, Germany) with ×200 magnification.

Image analysis

All images were analyzed using ImageJ software (National Institutes of Health, USA). A circular region of interests (ROI) of the standard size was manually placed in the center of the ischemic lesion on MRI parametric maps and microphotographs of anatomically matched LFB, BSI, NeuN, and Iba1-stained sections. The lesion was defined as hypointense on MPF maps and hyperintense on T_2 maps area that also showed abnormal LFB staining on a matched histological section. A similar ROI was placed at the symmetrical anatomic location in the contralateral hemisphere. The ROI size was chosen based on the smallest lesion observed in the entire animal sample. For sham-operated animals, ROIs were placed approximately in the center of the caudoputamen. LFB optical density (OD) was quantified from the intensity of the red channel on RGB images with background correction as previously described.[12,13] Axonal density was quantified from BSI-stained sections using the Otsu threshold method[36] in the ImageJ implementation described elsewhere.[37] Percentage of the total area of detected objects was used as a surrogate measure of axonal density.[37] The number of neurons was assessed as the count of NeuN-positive cells co-localized with DAPI within an ROI and normalized to 1 mm^2 area. Microglial activation was evaluated similarly using Iba1-labeled sections. Images of each type were analyzed by a single operator blinded to information about the time between surgery and imaging.

Statistical analysis

The differences between the ischemic lesions in the left hemisphere and the contralateral hemisphere were assessed using the paired *t*-test. The percentage changes (PC) in the measured MRI, histological, and immunohistochemical parameters were calculated as PC = (CL–IL)/CL × 100, where IL is a parameter value in the

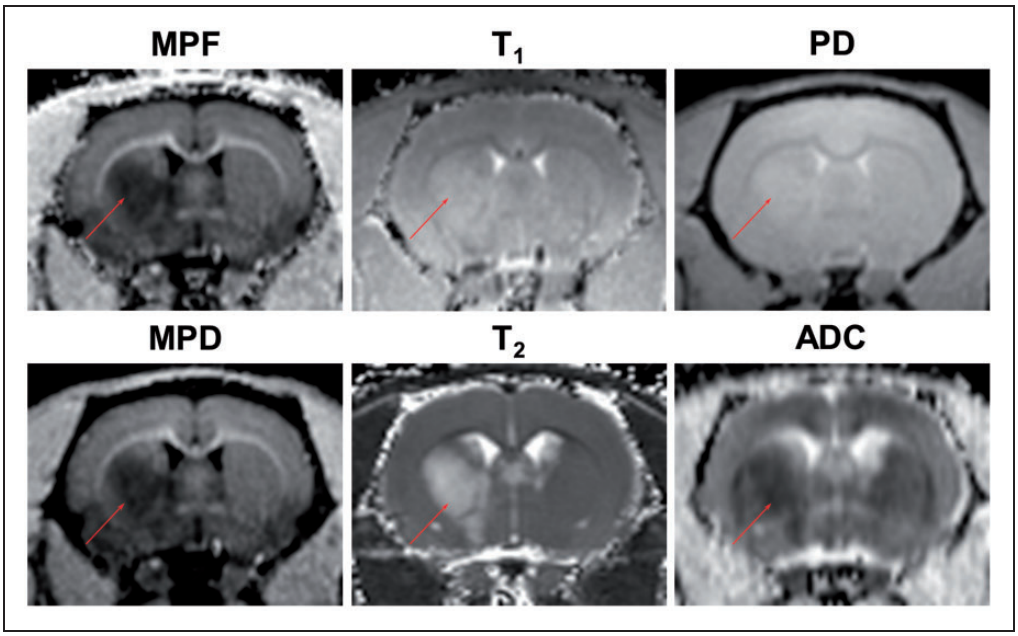

Figure 1. Example MRI parametric maps of the rat brain obtained on the first day after MCAO. Grayscale range corresponds to the following parameter ranges: 0–22% for MPF, 0–3000 ms for T_1, 0–110% for PD, 0–15% for MPD, 0–100 ms for T_2, and 0–2 × 10^{-3} mm^2/s for ADC. Arrows indicate the ischemic lesion.

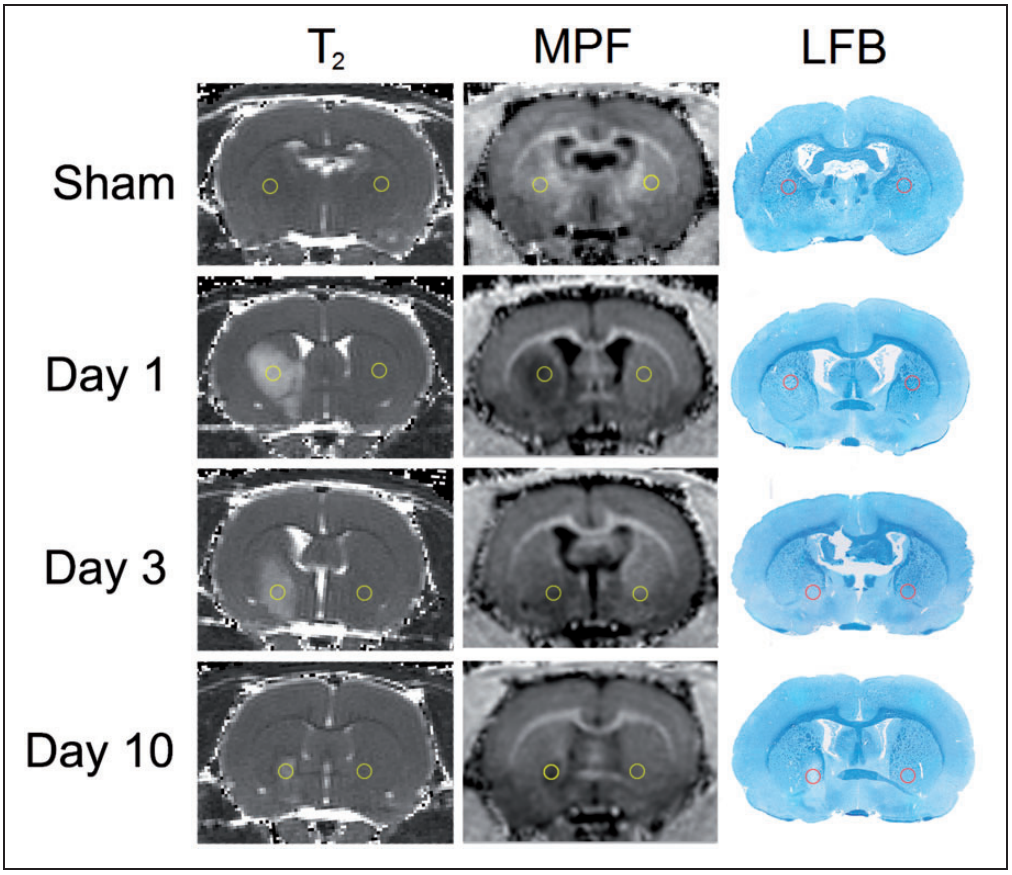

Figure 2. Examples of anatomically matched T_2 maps, MPF maps, and LFB-stained histological sections obtained from a sham-operated animal and animals studied on the 1st, 3rd, and 10th day after MCAO. Circles indicate ROIs used for parameter measurements in the ischemic lesion and contralateral anatomic region.

ischemic lesion and CL is a parameter value at the symmetrical location in the contralateral hemisphere. To assess relationships between demyelination and other histological and imaging variables, percentage changes in LFB optical density were compared to percentage changes in other variables in a series of analyses using a repeated-measures ANOVA model. In these analyses, the percentage change in LFB optical density was uniformly used as a reference standard reflecting an extent of demyelination, and all other variables were sequentially tested to identify distinctions or similarities across animal groups. The model included a group factor (1-, 3-, and 10-day groups), a repeated-measurement factor (LFB optical density and any other measured parameter), and their interaction followed by post hoc pairwise tests with Tukey correction for multiple comparisons. Associations between imaging and histological variables were assessed using the Pearson correlation coefficient (R). Additionally, multivariate regression models were tested using a stepwise variable elimination procedure to identify a combination of quantitative MRI parameters that could provide the best prediction of percentage changes in LFB optical density. Statistical analysis was carried out in Statistica software (StatSoft Inc, USA). All tests were two-tailed with significance level of $P < 0.05$.

Results

Quantitative MRI, histology, and immunohistochemistry of the ischemic lesions

Example quantitative MRI maps used in this study are shown in Figure 1. Ischemic lesions located in the striatum were clearly identifiable in all animals by both histological LFB staining and parametric MPF and T_2 mapping. Figure 2 exemplifies the appearance of lesions in the 1-, 3-, and 10-day animal groups on MPF and T_2 maps and LFB-stained sections along with ROIs used for parameter measurements. Figure 3 shows magnified views of the lesion and contralateral anatomic region on microphotographs of LFB- and BSI-stained and NeuN and Iba1 immunofluorescence-labeled sections corresponding to the locations presented in Figure 2. Microphotographs for a sham-operated animal demonstrate normal microscopic appearance of the striatum. According to LFB staining (Figure 3), on the first day after MCAO, the lesion

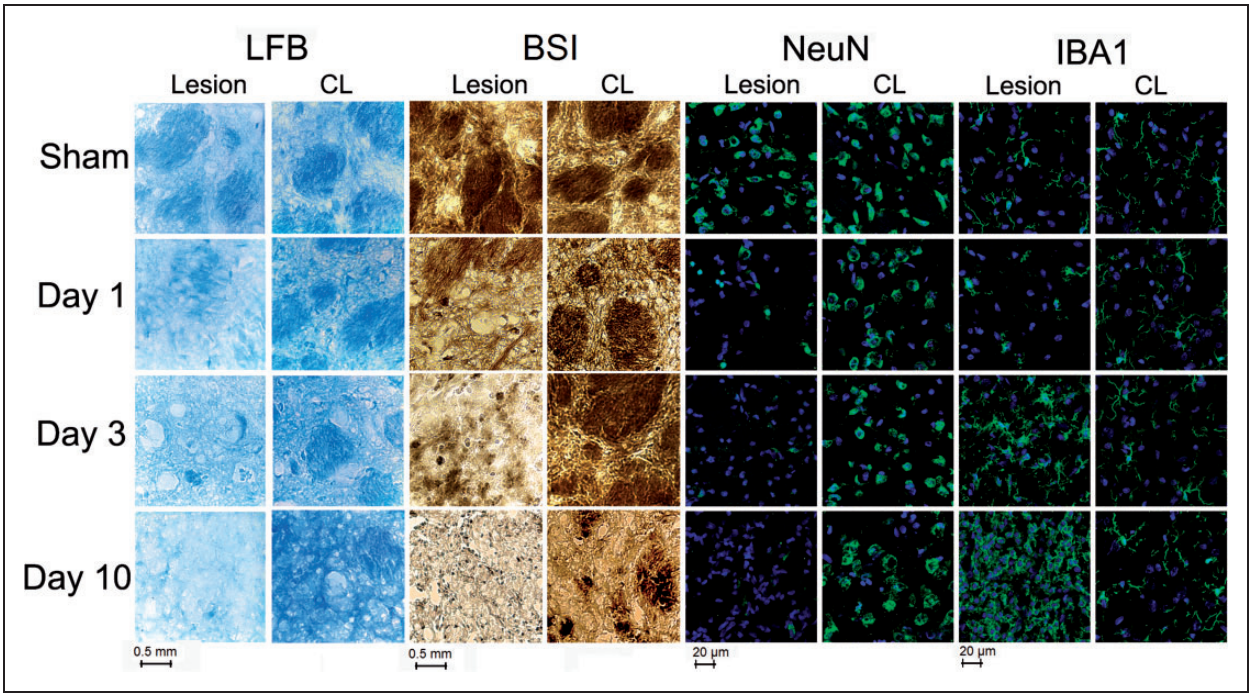

Figure 3. Magnified views of microphotographs of LFB- and BSI- stained and NeuN and Iba1 immunofluorescence-labeled histological sections obtained from a sham-operated animal and animals studied on the 1st, 3rd, and 10th day after MCAO. Microphotographs of ischemic lesions (or ipsilateral region in a sham-operated animal) and symmetric contralateral anatomic regions (CL) are from the same animals and anatomic locations, which are presented in Figure 2. In the immunofluorescence images of NeuN and Iba1-labeled sections, the green channel corresponds to NeuN-positive or Iba1-positive cells, and the blue channel depicts the nuclei labeled with DAPI.

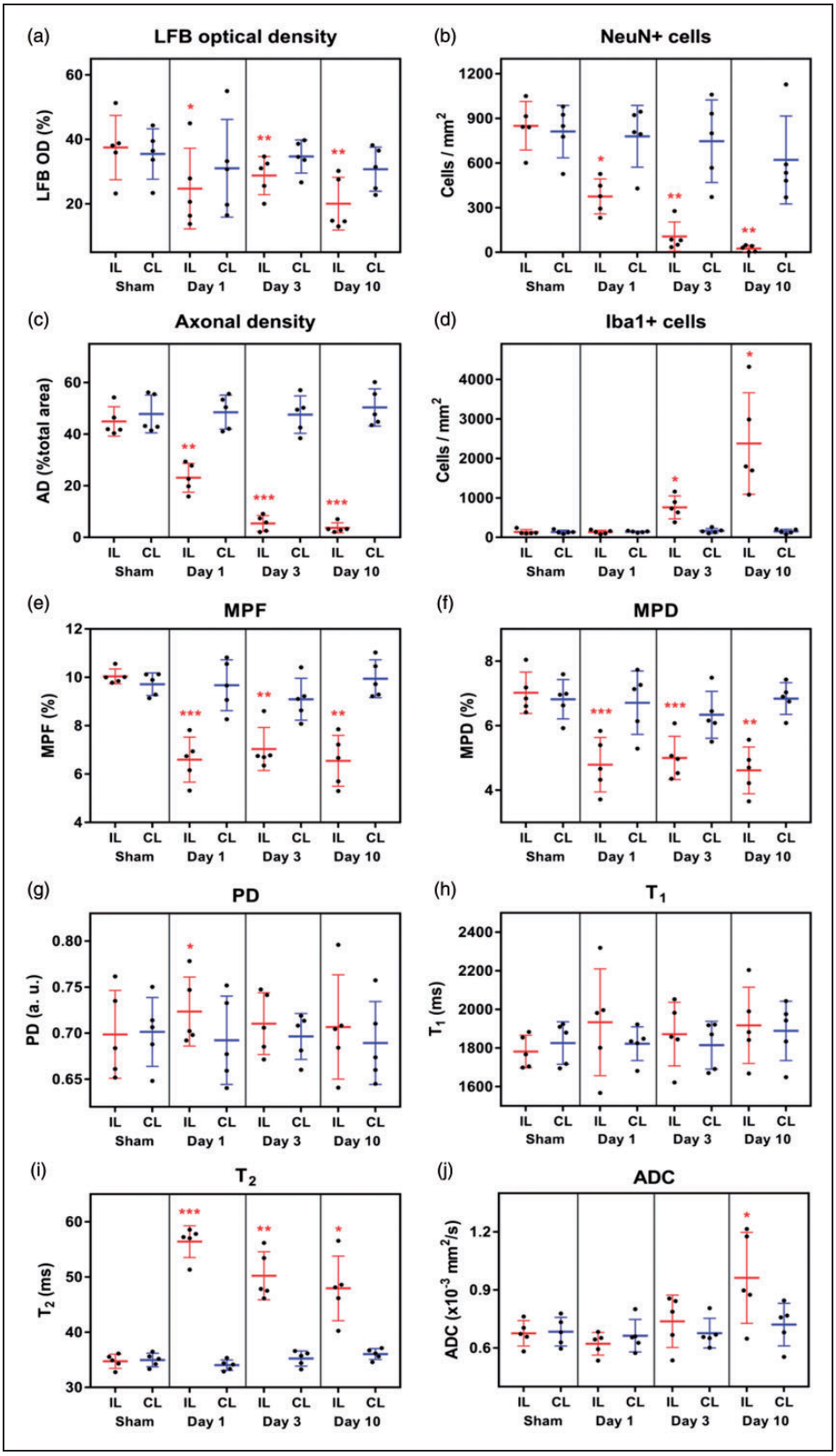

Figure 4. Scatterplots of quantitative MRI, histological, and immunohistochemical measurements across the groups of animals (sham-operated and 1, 3, and 10 days after MCAO) in the ischemic lesions or ipsilateral regions in sham-operated animals (IL) and symmetric contralateral regions (CL): (a) LFB optical density, (b) NeuN-positive cell count, (c) axonal density, (d) Iba1-positive cell count, (e) MPF, (f) MPD, (g) PD, (h) T_1, (i) T_2, and (j) ADC. Horizontal bars indicate mean values. Error bars correspond to standard deviations. Asterisks indicate significant differences between ipsilateral and contralateral measurements according to the paired *t*-test: $^{*}P < 0.05$, $^{**}P < 0.01$, $^{***}P < 0.001$.

showed myelin pallor in the ischemic core with enlarged interstitial spaces and without visible destruction of fiber tracts. In the 3-day group, marked vacuolization and partial destruction of myelin sheaths were observed. On the 10th day, the infarct core contained myelin debris and sparse fragments of residual myelin sheaths. BSI staining (Figure 3) showed progressive axonal loss from the 1st to the 10th day after the onset of ischemia with extensive disintegration of fiber bundles clearly visible on the 3rd and 10th days. NeuN immunofluorescence (Figure 3) demonstrated profound neuronal loss, which became almost complete in the 3- and 10-day groups. Iba1 immunofluorescence (Figure 3) identified prominent proliferation of activated microglia in the infarct core on the 3rd and, especially, 10th day after MCAO with characteristic changes in cellular morphology including an enlargement of soma and reduction of cell processes.

Quantitative MRI, histology, and immunohistochemistry measurements in the ischemic lesions and symmetric contralateral regions are summarized in Figure 4. No significant differences between the hemispheres were found in the sham-operated animals. LFB optical density, axonal density, and NeuN-positive cell count were significantly reduced relative to the contralateral hemisphere in all MCAO animal groups. Iba1-positive cell count was significantly increased in the 3- and 10-day groups. Among quantitative MRI variables, MPF and MPD were significantly reduced, and T_2 was significantly increased on the 1st, 3rd, and 10th day after MCAO. PD was significantly increased on the first day only. ADC demonstrated a significant increase in the 10-day group only. T_1 did not show significant distinctions in any group.

Percentage changes in MRI and histology parameters measured in the lesion relative to the contralateral hemisphere across MCAO groups are plotted in Figure 5. Detailed statistical report of a series of repeated-measures ANOVA tests comparing the percentage changes in LFB optical density used as a reference standard with other variables is available in online supplementary Table 1. Pairwise comparisons between LFB staining and other variables identified substantial similarity in the patterns of changes depicted by LFB, MPF, and MPD (Figure 5). Percentage changes in MPF and MPD significantly differed from those in LFB optical density on the 1st day after MCAO only ($P = 0.001$ and 0.035 for MPF and MPD, respectively) and did not differ on the 3rd and 10th days. A similar series of analyses revealed significant differences with respect to percentage changes in LFB optical density for the NeuN-positive cell count, axonal density, T_2, and PD (Figure 5) in all animal groups. Percentage changes in the Iba1-positive cell count significantly differed from changes in LFB optical density in the 3- and 10-day groups. T_1 percentage changes were significantly different from LFB optical density changes on the 1st and 10th days after MCAO,

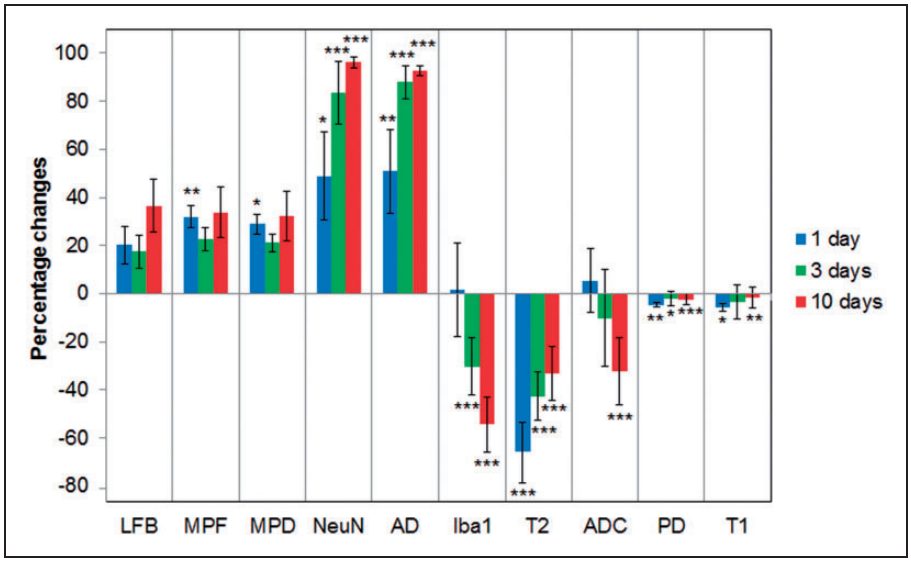

Figure 5. Mean percentage changes in quantitative MRI, histological, and immunohistochemical variables calculated for the ischemic lesion relative to the contralateral anatomical region across animal groups studied on the 1st, 3rd, and 10th day after MCAO. Note that percentage changes in Iba1-positive cell count are calculated after logarithmic transformation of raw cell count data due to extremely large scale of changes (see Figure 4(d)). Error bars correspond to standard deviations. Asterisks indicate significant differences as compared to percentage changes in LFB optical density for the same-day group according to repeated-measures ANOVA: $^{*}P < 0.05$, $^{**}P < 0.01$, $^{***}P < 0.001$.

but the difference on the 3rd day did not reach significance. ADC showed a significant difference in the 10th-day group only.

Associations between quantitative MRI and histology

Coefficients of correlations between percentage changes in imaging and histological variables are summarized in Table 1. Scatterplots of selected correlations along with linear regression models are presented in Figure 6. Among quantitative MRI parameters, only percentage changes in MPF and MPD significantly correlated with changes in LFB optical density (Table 1, Figure 6). Percentage changes in MPF and MPD did not significantly correlate with any other histological and immunohistochemical variable. Percentage changes in T_2 significantly correlated with changes in NeuN-positive cell count and axonal density. For ADC percentage changes, significant correlations were identified with percentage changes in NeuN- and Iba1-positive cell count and axonal density. Within the block of imaging variables, significant correlations were identified only between changes in MPF and MPD ($R = 0.98$, $P < 0.001$) and between changes in T_1 and PD ($R = 0.72$, $P = 0.002$). Among histological variables, significant correlations were found between axonal and neuronal loss ($R = 0.72$, $P = 0.002$) and between changes in LFB optical density and Iba1-positive cell count ($R = -0.55$, $P = 0.04$).

A series of regression analyses was performed to identify the combinations of quantitative MRI parameters enabling the best prediction of demyelination in the ischemic lesion as described by the LFB optical density. Percentage changes in either MPF or MPD appeared the best predictors of percentage changes in LFB optical density in the lesion within univariate models (Figure 6) and demonstrated very similar strengths of correlations ($R = 0.81$ and 0.82, respectively). Both models had

Table 1. Correlations between percentage changes in histological and MRI parameters.

Percentage changes	MPF	MPD	PD	T_1	T_2	ADC
LFB optical density	**0.81 (<0.001)**	**0.82 (<0.001)**	−0.24 (0.38)	−0.24 (0.39)	0.12 (0.67)	−0.48 (0.07)
NeuN+ cell count	−0.07 (0.80)	0.03 (0.92)	0.45 (0.09)	0.20 (0.47)	**0.68 (0.006)**	**−0.54 (0.04)**
Axonal density (% total area)	−0.14 (0.62)	−0.07 (0.80)	0.35 (0.20)	0.25 (0.36)	**0.65 (0.008)**	**−0.56 (0.03)**
Iba1+ cell count	−0.34 (0.21)	−0.39 (0.15)	−0.09 (0.75)	−0.17 (0.55)	−0.42 (0.12)	**0.74 (0.002)**

Note: Data are the Pearson correlation coefficients (R) with *P* values in parentheses. Significant correlations are highlighted in bold.

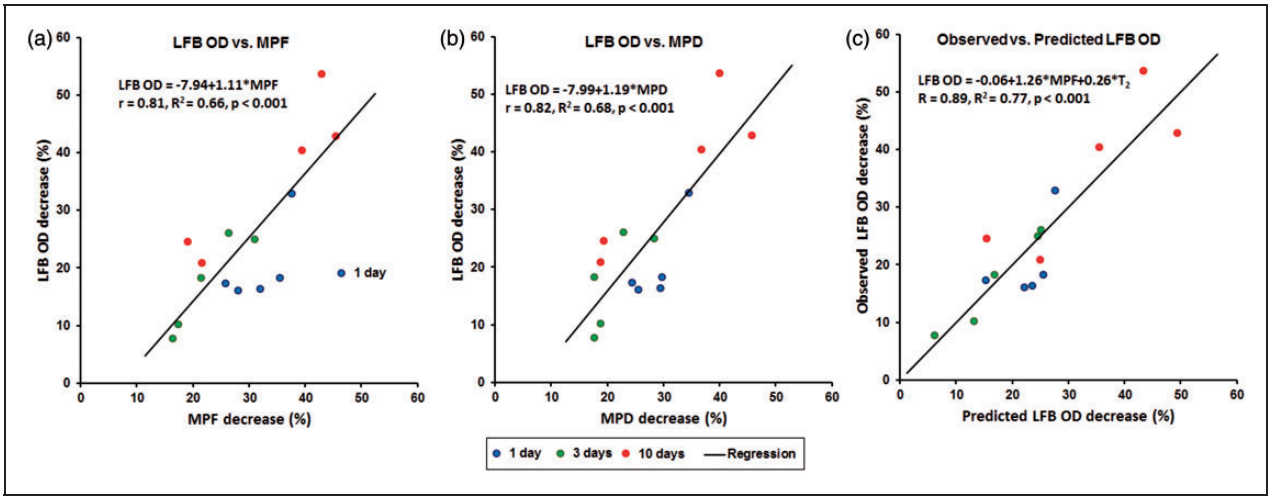

Figure 6. Linear regression plots of percentage changes in LFB optical density in the ischemic lesion relative to the symmetric contralateral anatomical region as a function of (a) percentage changes in MPF, (b) percentage changes in MPD, and (c) percentage changes in LFB optical density predicted using a bivariate regression model with percentage changes in MPF and T_2 as independent variables. Points represent color-coded experimental data for the 1st day (blue), 3rd day (green), and 10th day (red) groups.

non-significant intercept values, which, however, were substantially different from zero (−7.84% ($P = 0.26$) and −7.99% ($P = 0.25$) for the models with MPF and MPD, respectively). In the stepwise multivariate regression analyses, only percentage changes in MPF or MPD and T_2 were retained in the models as significant predictors of percentage changes in LFB optical density (Figure 6). Note that MPF and MPD were separately treated in these models to avoid collinearity problems. The resulting models provided significant improvement of R^2 compared to univariate models with R^2 change of 0.14 ($P = 0.02$) for the regression on percentage changes in MPF and T_2 and R^2 change of 0.10 ($P = 0.04$) for the regression on percentage changes in MPD and T_2. The structure of these models reflects the dominant effect of MPF or MPD and essentially similar behavior of changes in MPF and MPD as predictors of changes in LFB optical density with the following regression statistics: $R = 0.89$, adjusted $R^2 = 0.76$, $\beta(MPD) = 0.92$ ($P < 0.001$), and $\beta(T_2) = 0.38$ ($P = 0.02$) for the model including MPF and T_2; and $R = 0.88$, adjusted $R^2 = 0.74$, $\beta(MPD) = 0.90$ ($P < 0.001$), and $\beta(T_2) = 0.33$ ($P = 0.02$) for the model including MPD and T_2. In both bivariate models, intercept values were insignificant and very close to zero (−0.06% ($P = 0.99$) and 0.48% ($P = 0.94$) for the models with MPF and MPD, respectively).

Discussion

This study demonstrates the feasibility of non-invasive quantitative assessment of myelin damage in ischemic stroke and provides histological validation of the fast MPF mapping method as a myelin imaging tool at different stages of the lesion formation. Similar to previous studies of MPF mapping in the normal rat brain[13] and cuprizone-induced demyelination in mice,[12] we found close quantitative agreement between MPF and histologically determined myelin content in brain tissues. An important practical advantage of the fast MPF mapping method is its easy clinical translation confirmed by the recent MS and mTBI studies.[14,15] Based on the fastest to date MPF mapping technology utilizing synthetic reference reconstruction,[11,30] it is possible to design MRI protocols with a scan time of a few minutes suitable for clinical stroke studies.

A notable finding of this study is insensitivity of MPF to various pathological processes in the ischemic lesion, such as neuronal and axonal loss and inflammation, suggesting that changes in the myelin content provide the main pathological substrate of MPF changes. Myelin damage in stroke occurs due to several mechanisms. In the acute phase, intramyelinic edema disrupts the internal structure of the myelin sheath that histologically manifests as myelin pallor.[6] This process further advances to vacuole formation and sheath destruction followed by myelin debris clearance by microglia and macrophages.[4–6] In parallel, oligodendroglial injury also starts at the earliest stroke stage and prevents subsequent remyelination.[1,3,9] Secondary mechanisms of myelin loss include anterograde (Wallerian) and retrograde axonal degeneration, which occur in chronic stroke.[38,39] Our observations are in overall agreement with numerous studies that showed a decrease in the myelin content in the ischemic lesion from the first hours[1–3,6] after stroke in animal models. Furthermore, a weak but significant correlation between a decrease in LFB optical density and Iba1-positive cell proliferation probably reflects the role of inflammatory cascade in myelin degradation.[4–6] At the same time, the absence of correlation between MPF and proliferation of activated microglia suggests that MPF is mainly determined by the global changes in tissue composition at the levels of myelin and water content rather than specific cellular events potentially causing such changes. Similarly, neuroaxonal loss seems to cause a negligible effect on the tissue macromolecular content measured by MPF as compared to demyelination. Subtle changes in MPF associated with neural tissue cellularity also may be offset by the replacement of dying neurons, axons, and oligodendroglia with proliferating microglia. Although the loss of myelin, axons, and neuron occurs simultaneously in the infarct core, according to our data, these processes are characterized by different rates and degrees of completeness within the timeframe of our experiments. Particularly, demyelination seems to be a slower process as compared to neuronal and axonal loss, and the residual amount of myelin observed in the 10-day group appeared larger relative to the number of intact neurons and axons. While these discrepancies can be explained in terms of fundamentally different sensitivities of CNS tissue components to ischemia, some methodological aspects of the used histological techniques also should be taken into account. Specifically, LFB staining is a semi-quantitative technique which does not allow the absolute myelin content quantification. As most histological stains, it is subjected to limitations of background staining, uneven staining, and inherent variability of staining intensity due to various laboratory factors. The use of normalization to the contralateral hemisphere in our study to some extent alleviated these problems. LFB staining also may not distinguish between viable myelin and its debris based on the optical density measurements as long as the products of myelin breakdown retain the affinity to LFB.[40] Therefore, residual LFB staining in the infarct core may result in underestimation of an actual extent of demyelination in terms of the loss of functional myelinated fibers. As such, quantitative correlations with LFB optical density should be interpreted with caution, though the global similarity

between LFB staining and MPF maps has been reproducibly observed in this and previous studies.[12,13]

While MPF and LFB optical density demonstrated strong correlation, a discrepancy between these parameters on the first day after MCAO should be noted. An overestimation of myelin loss in acute stroke by MPF can be addressed to the confounding effect of edema due to increased water concentration. It was shown that water content in the injured hemisphere reaches maximum on the first day after transient MCAO.[41] The effect of edema on MPF can be quantitatively estimated as dilution of the macromolecular content. For example, an increase in regional water content by 10% (which is typical for the rat MCAO model[42,43]) would decrease an absolute MPF value approximately by 1% from a baseline value of 10%. In terms of percentage change, the 10% dilution effect completely explains the difference between MPF (~30%) and LFB optical density (~20%) seen in the first-day group (Figure 5). At the same time, MPF and histology provided nearly identical estimates of myelin loss at the latter stages of the lesion formation.

To further improve quantitative accuracy of MPF as a myelin biomarker in stroke, we tested two approaches to correct the effect of edema. One approach is based on the literature[34] and relies on the assumption that the combination of MPF and PD taken as the MPD parameter could be less sensitive to changes in the tissue water content. However, while the observed time course of PD changes is in agreement with water content changes in stroke,[42,43] this approach seems to be incapable of correcting for a possible dilution effect in MPF. It is also noticeable that the changes in PD observed in our study are highly consistent with earlier data in a rat stroke model,[44] where this parameter was elevated by about 5% at 24 h after MCAO, reached the maximum of around 10% at 48 h, and gradually decreased then. Our results showing a nearly identical behavior of MPF and MPD in univariate and multivariate regression models are in close agreement with the previous findings for acute multiple sclerosis lesions,[34] where both variables showed very similar temporal trajectories, and MPD did not provide any substantial correction for edema. To some extent, the above limitation of the PD correction technique could be addressed to the absence of the external standard and sophisticated techniques for coil sensitivity profiling, which are required for precise PD measurements[43] and were not used in our and the previous[34] studies. At the same time, improvements in accuracy of absolute PD quantitation are unlikely to change the above conclusions, because both studies utilized normalization to a similar location in the contralateral hemisphere. It also should be pointed out that absolute PD quantitation is rather impractical in the context of clinical translation due to the complexity of involved acquisition and processing procedures.

An alternative approach discovered in this work is based on the use of T_2 for the edema effect correction within a multiple regression model. Our results indicate that bivariate regression with MPF and T_2 as predictors enables accurate estimation of myelin density and eliminates any bias as indicated by the zero intercept in the regression equation. At the same time, this observation should be considered preliminary and taken with caution for the two reasons. First, this proof-of-concept study was not designed for precise multiple regression model testing, and therefore the sample size may be insufficient for drawing reliable conclusions from such regressions. Second, our results were obtained using an ultra-high-field MRI scanner and need to be revalidated for clinical field strengths. While MPF is independent of magnetic field, T_2 has a strong field dependence.[30] In view of the multicomponent nature of T_2 in tissues and different field dependences of these components,[30] T_2 measured in different magnetic fields may have different sensitivity to edema. Multi-echo T_2 measurements are also rather time-consuming for routine clinical use. For this reason, in the perspective of clinical translation, surrogate fast T_2 estimation techniques, such as a gradient and spin-echo approach[45] need to be tested. Alternatively, the strategies based on using T_1 instead of T_2 need to be evaluated owing to the fact that temporal trajectories of T_1 and T_2 changes in the ischemic lesion are substantially similar.[44] Being a part of the MPF mapping protocol,[10,11] T_1 mapping would not impose scan time penalties in this scenario. It also needs to be emphasized that a limited utility of T_1 for the characterization of the ischemic lesion demonstrated in our study should be attributed to the effect of T_1 convergence in ultra-high magnetic fields,[30] and therefore is not representative of T_1 behavior at clinical field strengths.

As a parallel outcome of this study, one should mention several significant correlations between imaging and histological variables, which are not related to the myelin content. Particularly, percentage changes in T_2 and the quantities of neurons and axons were positively correlated. Percentage changes in ADC negatively correlated with neuronal and axonal changes and positively with Iba1-positive cell count changes (Table 1). Note that in view of the uniform definition of percentage changes relative to the contralateral hemisphere used in this study, a negative change reflects an actual increase of a parameter in the lesion and vice versa. As such, the observed correlations suggest that T_2 decreases and ADC increases with a greater extent of neuronal and axonal loss and, additionally, ADC increases with proliferation of activated microglia in the infarct core. A

possible explanation of the observed trends may be related to the synchrony of processes of edema resolution, continuing neuroaxonal death, gliosis, inflammation, and necrosis, which cause rather complex changes in tissue water compartmentalization. The timeframe of our experiments corresponds to nearly monotonic trends of a decrease in T_2 and increase in ADC after reaching their maximal and minimal values, respectively, within 24 h after the onset of cerebral ischemia.[44,46] More specifically, our first observation point (1-day group) approximately matches the time of equalization of ADC related to the coincidence of cytotoxic and vasogenic edema.[44,46,47] Further increase in ADC is typically attributed to massive cell necrosis,[44,46,47] which is in agreement with the profound neuronal and axonal loss observed in our work. The decline in T_2 probably reflects a decrease in the tissue water content during vasogenic edema resolution from its peak value occurring around 24 h after ischemia.[44,46] It remains to be established in future studies how specific cellular events contribute into T_2 and ADC, and whether the above associations have further biological or clinical implications.

In conclusion, this study demonstrates that fast MPF mapping enables quantitative assessment of myelin damage in the MCAO model of ischemic stroke. Our results provide histological validation and methodological background for future clinical and preclinical applications of MPF as an imaging biomarker of demyelination in cerebral ischemia.

Funding

The author(s) disclosed receipt of the following financial support for the research, authorship, and/or publication of this article: The work was supported by the Russian Science Foundation, project No. 14-45-00040. Dr. Atochin received partial support for his activities from the Russian Science Foundation, project No. 17-15-01111.

Acknowledgements

The authors thank Ms. Svetlana Kildyaeva for proofreading the manuscript.

Declaration of conflicting interests

The author(s) declared no potential conflicts of interest with respect to the research, authorship, and/or publication of this article.

Authors' contributions

MYK, DNA, and VLY designed the study. MYK performed statistical analysis and wrote the manuscript. AAK and DNA were responsible for the development of the animal model. AEA and VLY performed MRI studies. AAK, MSK, and VYG performed image analysis. AAK and MSK performed immunohistochemical labeling. LRM performed histological processing and staining. MVS performed processing of MRI images. YAM performed tissue processing. VLY developed an MRI protocol and image processing software and critically revised the manuscript. All authors reviewed and approved the final version of the manuscript.

Supplementary material

Supplementary material for this paper can be found at the journal website: http://journals.sagepub.com/home/jcb

References

1. Dewar D, Underhill SM and Goldberg MP. Oligodendrocytes and ischemic brain injury. *J Cereb Blood Flow Metab* 2003; 23: 263–274.
2. Jing L, He Q, Zhang J-Z, et al. Temporal profile of astrocytes and changes of oligodendrocyte-based myelin following middle cerebral artery occlusion in diabetic and non-diabetic rats. *Int J Biol Sci* 2013; 9: 190–199.
3. Pantoni L, Garcia JH and Gutierrez JA. Cerebral white matter is highly vulnerable to ischemia. *Stroke* 1996; 27: 1641–1646.
4. Tanaka Y, Imai H, Konno K, et al. Experimental model of lacunar infarction in the gyrencephalic brain of the miniature pig. *Stroke* 2008; 39: 205–212.
5. Burda JE and Sofroniew MV. Reactive gliosis and the multicellular response to CNS damage and disease. *Neuron* 2014; 81: 229–248.
6. Han C-W, Lee K-H, Noh MG, et al. An experimental infarct targeting the internal capsule: histopathological and ultrastructural changes. *J Pathol Transl Med* 2017; 51: 292–305.
7. Zhou J, Zhuang J., Li J, et al. Long-term post-stroke changes include myelin loss, specific deficits in sensory and motor behaviors and complex cognitive impairment detected using active place avoidance. *PLoS ONE* 2013; 8: e57503.
8. Zhang ZG and Chopp M. Oligodendrogenesis after cerebral ischaemia and traumatic brain injury. *EMJ Neurol* 2013; 1: 26–31.
9. McIver SR, Muccigrosso M, Gonzales ER, et al. Oligodendrocyte degeneration and recovery after focal cerebral ischemia. *Neuroscience* 2010; 169: 1364–1375.
10. Yarnykh VL. Fast macromolecular proton fraction mapping from a single off-resonance magnetization transfer measurement. *Magn Reson Med* 2012; 68: 166–178.
11. Yarnykh VL. Time-efficient, high-resolution, whole brain three-dimensional macromolecular proton fraction mapping. *Magn Reson Med* 2016; 75: 2100–2106.
12. Khodanovich MYu, Sorokina IV, Glazacheva VYu, et al. Histological validation of fast macromolecular proton fraction mapping as a quantitative myelin imaging method in the cuprizone demyelination model. *Sci Rep* 2017; 7: 46686.
13. Underhill HR, Rostomily RC, Mikheev AM, et al. Fast bound pool fraction imaging of the in vivo rat brain: association with myelin content and validation in the C6 glioma model. *Neuroimage* 2011; 54: 2052–2065.
14. Yarnykh VL, Bowen JD, Samsonov A, et al. Fast whole-brain three-dimensional macromolecular proton fraction

mapping in multiple sclerosis. *Radiology* 2015; 274: 210–220.
15. Petrie EC, Cross DJ, Yarnykh VL, et al. Neuroimaging, behavioral, and psychological sequelae of repetitive combined blast/impact mild traumatic brain injury in Iraq and Afghanistan war veterans. *J Neurotrauma* 2014; 31: 425–436.
16. Ou X, Sun SW, Liang HF, et al. The MT pool size ratio and the DTI radial diffusivity may reflect the myelination in shiverer and control mice. *NMR Biomed* 2009; 22: 480–487.
17. Janve VA, Zu Z, Yao S-Y, et al. The radial diffusivity and magnetization transfer pool size ratio are sensitive markers for demyelination in a rat model of type III multiple sclerosis (MS) lesions. *Neuroimage* 2013; 74: 298–305.
18. Samsonov A, Alexander AL, Mossahebi P, et al. Quantitative MR imaging of two-pool magnetization transfer model parameters in myelin mutant shaking pup. *Neuroimage* 2012; 62: 1390–1398.
19. Thiessen JD, Zhang Y, Zhang H, et al. Quantitative MRI and ultrastructural examination of the cuprizone mouse model of demyelination. *NMR Biomed* 2013; 26: 1562–1581.
20. Ordidge RJ, Helpern JA, Knight RA, et al. Investigation of cerebral ischemia using magnetization transfer contrast (MTC) MR imaging. *Magn Reson Imaging* 1991; 9: 895–902.
21. Ewing JR, Jiang Q, Boska, et al. T1 and magnetization transfer at 7 Tesla in acute ischemic infarct in the rat. *Magn Reson Med* 1999; 41: 696–705.
22. Mäkelä HI, Kettunen MI, Gröhn OH, et al. Quantitative T(1rho) and magnetization transfer magnetic resonance imaging of acute cerebral ischemia in the rat. *J Cereb Blood Flow Metab* 2002; 22: 547–558.
23. Pendlebury ST, Lee MA, Blamire AM, et al. Correlating magnetic resonance imaging markers of axonal injury and demyelination in motor impairment secondary to stroke and multiple sclerosis. *Magn Reson Imaging* 2000; 18: 369–378.
24. Tourdias T, Dousset V, Sibon I, et al. Magnetization transfer imaging shows tissue abnormalities in the reversible penumbra. *Stroke* 2007; 38: 3165–3171.
25. Sibon I, Tourdias T, Felix S, et al. Magnetisation transfer parameters and stroke outcome. *J Clin Neurosci* 2015; 22: 1012–1017.
26. Lin YC, Daducci A, Meskaldji DE, et al. Quantitative analysis of myelin and axonal remodeling in the uninjured motor network after stroke. *Brain Connect* 2015; 5: 401–412.
27. Dousset V, Grossman RI, Ramer KN, et al. Experimental allergic encephalomyelitis and multiple sclerosis: lesion characterization with magnetization transfer imaging. *Radiology* 1992; 182: 483–491.
28. Sled JG and Pike GB. Quantitative imaging of magnetization transfer exchange and relaxation properties in vivo using MRI. *Magn Reson Med* 2001; 46: 923–931.
29. Yarnykh VL. Pulsed Z-spectroscopic imaging of cross-relaxation parameters in tissues for human MRI: theory and clinical applications. *Magn Reson Med* 2002; 47: 929–939.
30. Naumova AV, Akulov AE, Khodanovich MY, et al. High-resolution three-dimensional macromolecular proton fraction mapping for quantitative neuroanatomical imaging of the rodent brain in ultra-high magnetic fields. *Neuroimage* 2016; 147: 985–993.
31. Atochin DN, Yuzawa I, Li Q, et al. Soluble guanylate cyclase $\alpha 1\beta 1$ limits stroke size and attenuates neurological injury. *Stroke* 2010; 41: 1815–1819.
32. Skinner TE and Glover GH. An extended two-point Dixon algorithm for calculating separate water, fat, and B0 images. *Magn Reson Med* 1997; 37: 628–630.
33. Yarnykh VL. Actual flip-angle imaging in the pulsed steady state: a method for rapid three-dimensional mapping of the transmitted radiofrequency field. *Magn Reson Med* 2007; 57: 192–200.
34. Giacomini PS, Levesque IR, Ribeiro L, et al. Measuring demyelination and remyelination in acute multiple sclerosis lesion voxels. *Arch Neurol* 2009; 66: 375–381.
35. Paxinos G and Watson C. *The rat brain in stereotaxic coordinates*, 6th ed. San Diego: Academic Press, 2007.
36. Otsu N. Threshold selection method from gray-level histograms. *IEEE Transac Syst Man Cybernet* 1979; 9: 62–66.
37. Kneynsberg A, Collier TJ, Manfredsson FP, et al. Quantitative and semi-quantitative measurements of axonal degeneration in tissue and primary neuron cultures. *J Neurosci Methods* 2016; 266: 32–41.
38. Qin W, Zhang M, Piao Y, et al. Wallerian degeneration in central nervous system: dynamic associations between diffusion indices and their underlying pathology. *PLoS One* 2012; 7: e41441.
39. Hinman JD. The back and forth of axonal injury and repair after stroke. *Curr Opin Neurol* 2014; 27: 615–623.
40. Schmidt RE. Diseases of CNS myelin. In: Nelson JS, Mena H, Parisi JE, et al. (eds) *Principles and practice of neuropathology*, 2nd ed. New York: Oxford University Press, 2003, pp.246–266.
41. Slivka A, Murphy E and Horrocks L. Cerebral edema after temporary and permanent middle cerebral artery occlusion in the rat. *Stroke* 1995; 26: 1061–1066.
42. Young W, Rappaport ZH, Chalif DJ, et al. Regional brain sodium, potassium, and water changes in the rat middle cerebral artery occlusion model of ischemia. *Stroke* 1987; 18: 751–759.
43. Lin W, Venkatesan R, Gurleyik K, et al. An absolute measurement of brain water content using magnetic

resonance imaging in two focal cerebral ischemic rat models. *J Cereb Blood Flow Metab* 2000; 20: 37–44.
44. Knight RA, Dereski MO, Helpern JA, et al. MRI assessment of evolving focal cerebral ischemia: comparison with histopathology in rats. *Stroke* 1994; 25: 1252–1262.
45. Sprinkart AM, Luetkens JA, Träber F, et al. Gradient Spin Echo (GraSE) imaging for fast myocardial T2 mapping. *J Cardiovasc Magn Reson* 2015; 17: 92.
46. Welch KM, Windham J, Knight RA, et al. A model to predict the histopathology of human stroke using diffusion and T2-weighted magnetic resonance imaging. *Stroke* 1995; 26: 1983–1989.
47. Pierpaoli C, Righini A, Linfante I, et al. Histopathologic correlates of abnormal water diffusion in cerebral ischemia: diffusion-weighted MR imaging and light and electron microscopic study. *Radiology* 1993; 189: 439–448.